ERDC/CRREL SR-22-1

US Army Corps
of Engineers®
Engineer Research and
Development Center

ERDC
ENGINEER RESEARCH & DEVELOPMENT CENTER

Extreme Terrain Research, "Forecasting EO/IR Extinction Characteristics for Active and Passive Optical Systems"

The Blowing Snow Hazard Assessment and Risk Prediction Model

A Python Based Downscaling and Risk Prediction for Snow Surface Erodibility and Probability of Blowing Snow

Theodore W. Letcher, Sandra L. LeGrand,
and Chris Polashenski

March 2022

Cold Regions Research
and Engineering Laboratory

Approved for public release; distribution is unlimited.

The U.S. Army Engineer Research and Development Center (ERDC) solves the nation's toughest engineering and environmental challenges. ERDC develops innovative solutions in civil and military engineering, geospatial sciences, water resources, and environmental sciences for the Army, the Department of Defense, civilian agencies, and our nation's public good. Find out more at www.erdc.usace.army.mil.

To search for other technical reports published by ERDC, visit the ERDC online library at https://erdclibrary.on.worldcat.org/discovery.

ERDC/CRREL SR-22-1
March 2022

The Blowing Snow Hazard Assessment and Risk Prediction Model

A Python Based Downscaling and Risk Prediction for Snow Surface Erodibility and Probability

Theodore W. Letcher, Sandra L. LeGrand, and Chris Polashenski

Cold Regions Research and Engineering Laboratory
U.S. Army Engineer Research and Development Center
72 Lyme Road
Hanover, NH 03755

Final report

Approved for public release; distribution is unlimited.

Prepared for Assistant Secretary of the Army for Acquisitions, Logistics, and Technology
103 Army Pentagon
Washington, DC 20314-1000

Under Project 479378, Extreme Terrain Research, "Forecasting EO/IR Extinction Characteristics for Active and Passive Optical Systems" under Work Item BKCH02, Funding Account Number U4365315

Abstract

Blowing snow is an extreme terrain hazard causing intermittent severe reductions in ground visibility and snow drifting. These hazards pose significant risk to operations in snow-covered regions. While many ingredients-based forecasting methods can be employed to predict where blowing snow is likely to occur, there are currently no physically based tools to predict blowing snow from a weather forecast. However, there are several different process models that simulate the transport of snow over short distances that can be adapted into a terrain forecasting tool. This report documents a downscaling and blowing-snow prediction tool that leverages existing frameworks for snow erodibility, lateral snow transport, and visibility, and applies these frameworks for terrain prediction. This tool is designed to work with standard numerical weather model output and user-specified geographic models to generate spatially variable forecasts of snow erodibility, blowing snow probability, and deterministic blowing-snow visibility near the ground. Critically, this tool aims to account for the history of the snow surface as it relates to erodibility, which further refines the blowing-snow risk output. Qualitative evaluations of this tool suggest that it can provide more precise forecasts of blowing snow. Critically, this tool can aid in mission planning by downscaling high-resolution gridded weather forecast data using even higher resolution terrain dataset, to make physically based predictions of blowing snow.

DISCLAIMER: The contents of this report are not to be used for advertising, publication, or promotional purposes. Citation of trade names does not constitute an official endorsement or approval of the use of such commercial products. All product names and trademarks cited are the property of their respective owners. The findings of this report are not to be construed as an official Department of the Army position unless so designated by other authorized documents.

DESTROY THIS REPORT WHEN NO LONGER NEEDED. DO NOT RETURN IT TO THE ORIGINATOR.

Contents

Figures and Tables

Figures

Tables

Preface

This study was conducted for the Assistant Secretary of the Army for Acquisition, Logistics, and Technology (ASA-ALT) under Project 479378, Extreme Terrain Research, "Forecasting EO/IR Extinction Characteristics for Active and Passive Optical Systems." The technical monitor was Dr. Theodore Letcher, ERDC Cold Regions Research and Engineering Laboratory (CRREL).

The work was performed by the Terrestrial and Cryospheric Sciences Branch (CEERD-RRG) of the Research and Engineering Division (CEERD-RR), U.S. Army Engineer Research and Development Center, Cold Regions Research and Engineering Laboratory (ERDC-CRREL). At the time of publication, Dr. John Weatherly was Chief, RRG, and Dr. George Calfas was Chief, RR. The Acting Deputy Director of CRREL was Mr. Bryan E. Baker, and the Director was Dr. Joseph L. Corriveau.

COL Teresa A. Schlosser was the Commander of ERDC, and Dr. David W. Pittman was the Director.

1 Introduction

Blowing snow events often occur with little warning, presenting substantial risks to operational safety, mobility, infrastructure, and intelligence. Re-suspended snow can generate hazardous visibility conditions depending on ambient weather and lighting. Further, persistent blowing snow can accumulate into large snowdrifts and change the local terrain characteristics. These risks are particularly relevant for routine and special operations in mountainous and cold regions. For example, blowing snow can impair soldier movement in mountainous terrain and restrict the use of aviation support, but it can also be turned into an advantage in conducting attacks and concealing movement (e.g., ATP 3-90.97 2016). Despite these hazards, current operational standards for assessing blowing snow risks are minimal.

Existing blowing snow predictions are usually qualitative and emerge from forecaster analyses of environmental conditions or derive from "ingredients-based" assumptions (e.g., if strong winds and fresh snow are present, assume blowing snow risk). While these approaches can offer advanced warnings about potentially dangerous conditions, several Army applications like sensor performance assessment, autonomous system communication, load-bearing applications, and route planning require accurate snow transport estimates. Furthermore, while blowing snow is not a hazard unique to mountain regions, it is a common occurrence in regions with high relief where the blowing snow risk varies over extremely short distances. This poses an additional challenge to forecasters as current weather forecast models do not adequately resolve small-scale terrain features that determine the spatial variability of risk.

To address this shortfall, researchers from the U.S. Army Engineer Research and Development Center (ERDC) developed an advanced blowing snow risk assessment capability called the Blowing Snow Hazard Assessment and Risk Prediction (BSHARP) model. BSHARP generates 2-D maps highlighting snow surface erodibility, blowing snow risk, and visibility degradation. BSHARP is unique as it is capable of downscaling gridded numerical weather prediction (NWP) model output to higher-resolution digital elevation models (DEMs) to obtain greater forecast spatial resolution. Additionally, BSHARP accounts for the accumulated

effects of wind, temperature, and precipitation on the susceptibility of a snowpack to wind erosion.

BSHARP uses a three-tiered approach to assess risk. The 1st tier assesses the snow surface erodibility, the 2nd tier is a probabilistic assessment of the blowing snow risk determined by the snowpack erodibility (from tier 1), and the forecast wind speed. The 3rd and final tier is a deterministic forecast of visibility at 2 m above ground level (AGL) as determined by known optical properties of blowing snow.

This capability is demonstrated over Alaska because Alaska is frequently impacted by blowing snow and has a dedicated high-resolution ($\Delta x = 3km$) operational NWP model run by the National Oceanic and Atmospheric Administration (NOAA).

In this report, the authors detail the most salient features of BSHARP and provide a selection of examples of simulated risk over Alaska.

1.1 Background

Researchers have devoted substantial effort to better understanding and simulating aeolian (i.e., wind-driven) processes, and numerous studies have investigated blowing snow in both environmental and laboratory settings (e.g., Schmidt 1980; Pomeroy and Gray 1990; Nemoto and Nishimura 2004). Within the numerical modeling community, most aeolian transport schemes incorporate two fundamental transport modes: 1) saltation, which occurs within the lowest several decimeters above the ground, and 2) turbulent suspension, which represents the transport of surface material from the saltation layer into the atmospheric boundary layer. While there is no hard delineation between the two processes, generally particles in saltation follow a single parabolic trajectory back to the earth surface, while those in suspension experience complex trajectories with multiple upward turbulent lofting events. This designation is a practice common to both blowing soil and blowing snow numerical parameterizations. These simulated processes can be generally described as follows: In the saltation process, larger particles are entrained into the near-surface airflow by ground-level turbulence once the surface wind stress exceeds the friction binding the particle to the surface. These particles accumulate momentum from the wind and collide once again into the surface where they can eject additional particles into the flow – energy transfer in this way is considerably more effective than pure wind

shear, especially at ejecting (or creating) small particles. Some fraction of the ejected particles can then be entrained out of the surface layer and into the atmospheric boundary layer.

By assuming uniform snow surface erodibility, the blowing snow forecast reduces entirely to a nonlinear relation with windspeed forecast. However, in summary of blowing snow research, Pomeroy et al. (1993) note that blowing snow can initiate at windspeeds as low as approximately 3.5 ms^{-1} or can be restricted until windspeeds exceed approximately 23 ms^{-1}, a range of windspeeds that encompasses the majority of climatological conditions. Numerous studies have focused on better understanding surface erodibility both for soil and for snow. Typically, surface erodibility is quantified using a single parameter describing the threshold friction speed of the surface (u_{*t}). While this single parameter is almost certainly not a comprehensive assessment of surface erodibility, it is a convenient metric from a numerical modeling perspective as it casts surface erodibility in terms of a familiar meteorological variable: friction speed (u_*). For soils, u_{*t} is parameterized as a simple function of particle size, often with applied empirical corrections for soil moisture and surface vegetation or roughness (e.g., Kok 2012 and references within). However, simplified force balance constructs (e.g., Schmidt 1980; He and Ohara 2019) indicate that, unlike dust, snow surface erodibility is more related to the strength and number of interparticle bonds, rather than particle size. Therefore, unlike soil, snow surface erodibility is a complicated function of the snow particle temperature, size, shape, and snow surface bulk density. Since all of these properties change over time as the snowpack is exposed to variable wind, temperature, and radiation conditions, snow surface erodibility is difficult to predict. As a result, in contrast to soil transport parameterizations that generally treat u_{*t} in a consistent manner, the numerous physics-based blowing-snow parameterizations described in the literature treat u_{*t} in very different ways. These range from the simple, which treat u_{*t} as a time and space invariant constant (e.g., Liston and Sturm 1998; Kang et al. 2018) to the moderately complex that treat it as a function of varying snow temperature or density (Li and Pomeroy 1999; Déry and Yau 1999; Liston et al. 2007), to the highly complex which treat it as a function of varying density, size, and shape, all of which are evolved in physics-based ways as well (e.g., Vionnet et al. 2012; 2013; 2014).

While a majority of blowing-snow parameterizations are implemented to simulate and predict snow transport on scales of 10-100 m, a few studies

have adapted some aspects of blowing-snow prediction into mesoscale (1-100km) weather models to predict blowing-snow occurrence or visibility reductions (e.g., Bychova et al. 2018; Tanji and Inatsu 2019). However, the parameterizations implemented in these studies do not use the comprehensive start-to-finish parameterizations implemented in snow transport models, nor do they account for snowpack history and erodibility in a robust way.

BSHARP leverages the parameterizations developed from the laboratory, field, and modeling studies described above in combination with a downscaling procedure of moderate complexity to produce a 1km blowing snow risk forecast based on high resolution NWP output that uses the sophisticated physically based u_{*t} parameterization described in Vionnet et al. 2012; 2013; 2014.

1.2 Objective

The primary objective of this report is to document and demonstrate the initial release (version 1.0) of BSHARP. Here, we outline procedures used in BSHARP to:

1. Create a 1km resolution meteorological forcing dataset from coarser-resolution NWP data using moderate complexity downscaling techniques.

2. Couple snow aging and u_{*t} parameterizations described in Vionnet et al. (2012; 2013; 2014) to the resulting downscaled forcing dataset to generate snow erodibility maps.

3. Produce blowing snow risk assessments and blowing snow visibility reduction forecasts using parameterizations presented in Pomeroy and Gray (1990), Pomeroy et al. (1993), and Pomeroy and Male (1988).

4. Condense the resultant blowing snow risk assessments stored into date stamped Geotiff format for easy incorporation into Geographic Information System (GIS) software.

1.3 Approach

BSHARP V 1.0 modifies the snow-aging parameterizations designed for the multi-layer Crocus snow model to work with the simple zero-layer snow model used as part the North American Mesoscale (NAM) model. The BSHARP code is written in the Python programming language to take advantage of Python's large user base, readability, and freely available libraries that handle NWP and Geographic Information System (GIS) data formats. BSHARP is designed as a stand-alone package that can be called within separate Python scripts providing greater end-user flexibility. The following report documents the BSHARP framework. An additional appendix is provided that focuses on the technical software aspects of BSHARP and serves as a basic user guide.

2 Data and Methods

2.1 North American Mesoscale model Alaska

The NAM modeling system Alaska nest is a high-resolution meteorological forecast model that covers the state of Alaska. The Alaska Nest is a fully compressible non-hydrostatic model gridded at 3-km horizontal grid-spacing nested within the coarser (12-km resolution) NAM, which covers the entirety of North America. It uses the Weather Research and Forecast (WRF) Nonhydrostatic Mesoscale Model (NMM) dynamic core to simulate atmospheric motion. The vertical grid structure follows a hybrid sigma-pressure coordinate system. The microphysical parameterization is the Ferrier-Aligo, which tracks the production, advection, and deposition of cloud-water, cloud-ice, rain-water, and snow/graupel-ice (Aligo et al. 2014). Atmospheric shortwave and longwave radiation are parameterized with the Rapid Radiative Transfer Model (RRTM). The NAM is coupled to the surface using the Noah Land-Surface Model (LSM). The model output is post-processed and output to the 3-km resolution National Digital Forecast Database (NDFD). The vertical output is interpolated to 42 pressure levels ranging from 1000-to-10mb with a vertical resolution of approximately 25mb, providing a high-resolution picture of the atmospheric vertical structure. In addition to vertical and horizontal interpolation, the post-processing also generates large number of diagnostic variables from the atmospheric data relevant to weather forecasters. Post-processed NAM forecast output is available at hourly time-resolution out to 60 hr from model initialization. The model is run 4x daily and the output is publicly accessible from NOAA.

The model is reinitialized at the four synoptic times (00, 06, 12, 18 UTC) using the NAM Data Assimilation System (NDAS) to update the initial atmospheric state using available observations. Snow is updated in the model once daily at 06 UTC from the National Snow and Ice Data Center (NSIDC) snow cover analysis and Air Force Weather Agency (AFWA) snow depth analysis with an assumed 5:1 snow-to-liquid volume ratio. The NSIDC snow cover analysis is a binary (yes/no) 4-km resolution product that is used to add or remove snow such that the model snow cover is equivalent to the NSIDC product. The AFWA snow depth analysis is a 23-km resolution gridded snow depth product that determines snow depth and SWE at model grid-cells classified as snow cover. While these observations of snow cover and snow depth are imperfect, they help

ensure that the snow cover within the NAM is likely representative of the area of true snow cover over Alaska in most instances.

2.2 Meteorological downscaling

In the context of meteorology and climatology, "downscaling" has many different connotations, but generally refers to the translation of coarse-resolution gridded atmospheric data to a higher resolution grid using a physical or statistical relationship. There are several methods to downscale meteorological data, including nesting a high-resolution atmospheric model within a coarse model (dynamic downscaling: e.g., Liu et al. 2016), using known statistical relationships between coarse gridded data and observations (statistical downscaling: e.g., Wilby et al. 1998), and using mean physical relationships between sub-model-grid static terrain and land cover properties to match coarse model data to the finer DEM grid (terrain downscaling: Steinacker et al. 2006).

Terrain downscaling has the greatest impact in regions where there is substantial sub-grid terrain variability and is most accurate when the atmospheric model being downscaled is gridded at high enough resolution to resolve the majority of terrain-atmospheric interactions that influence atmospheric motion on the mesoscale (~O(<10km)). In determining whether or not terrain downscaling is good solution to a given problem, one must consider the spatial scale of the terrain (i.e., narrow vs. wide), the meteorological phenomenon of interest (e.g., turbulence vs. precipitation), and the model resolution. While 3-km horizontal resolution is too coarse to capture atmospheric motion at the scales of sharp individual mountain peaks and ridges, the effects of the broader mountain ranges on the atmosphere, and specifically, temperature, precipitation, and wind are well-resolved. More precision can then be obtained by downscaling these variables using known relationships between elevation and temperature, precipitation, and wind.

2.2.1 Digital Elevation Model (DEM)

While the downscaling methods described here are adaptable to any DEM, to demonstrate BSHARP in an operational environment, we use the Shuttle Radar Topography Mission (SRTM) 30 arc-second (~1-km) resolution DEM (Farr et al. 2007). We choose the 30 arc-second resolution DEM as it will provide substantially greater spatial detail without significantly

compromising accuracy or producing exorbitant computational expense. The terrain of the test domain over Alaska is presented in Figure 1.

Figure 1. Terrain from the Shuttle Radar Topography Mission (km ASL).

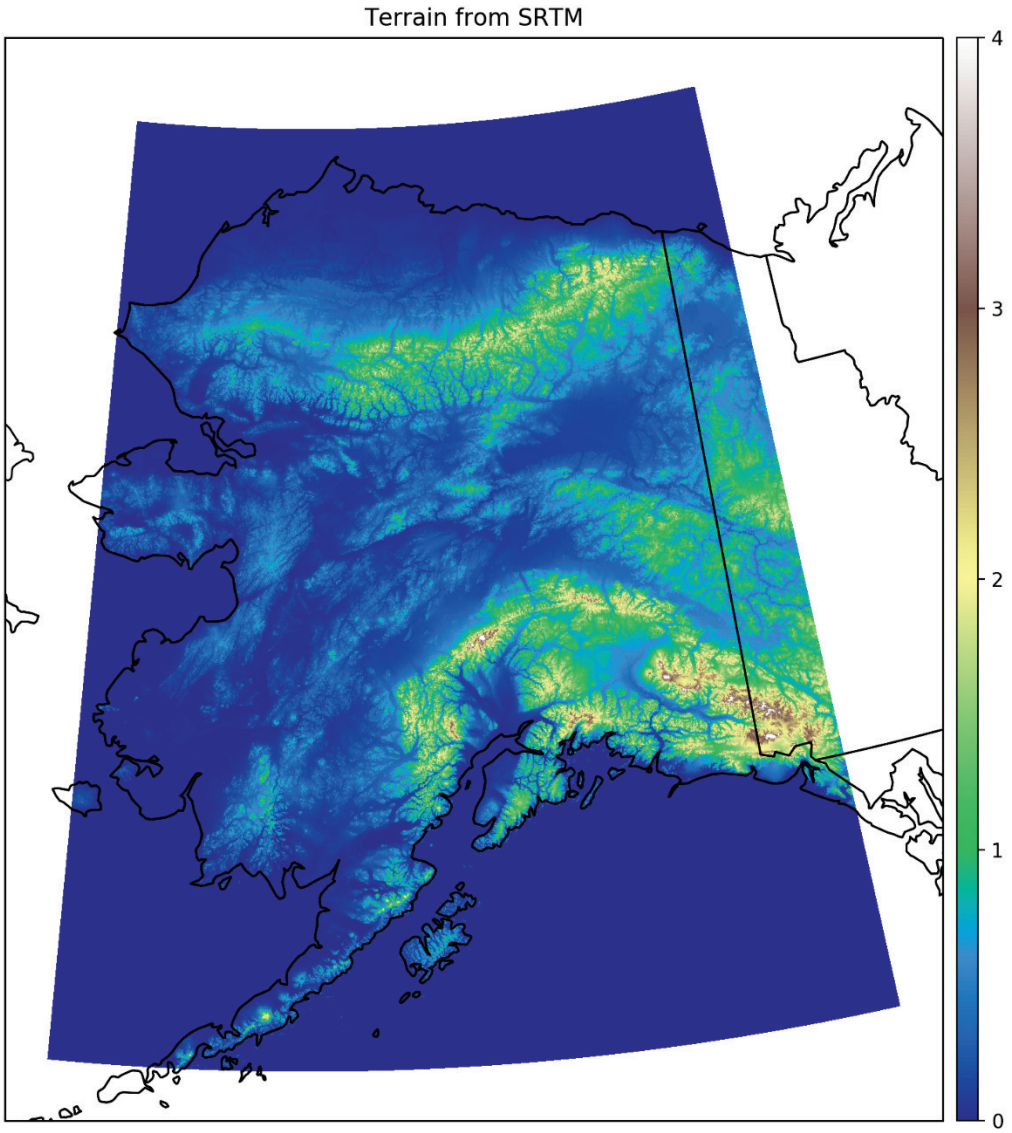

2.2.2 Temperature downscaling

Temperature is, arguably, the most critical variable to downscale accurately as it has a strong influence on the rain/snow partitioning, which critically alters snow erodibility. It also has an outsized impact on the physical characteristics of fresh snow and snow aging. There are several ways to downscale temperature ranging from simple solutions (e.g.,

assuming a fixed atmospheric lapse-rate [Liston and Elder 2006]) to the complex (e.g., computing the downscaled atmospheric volume and computing the effects of surface heating and cooling on the volume temperature [Steinacker et al. 2006]). The former is too simplistic and inaccurate for most applications (e.g., Minder et al. 2010), and generally is used only in situations when vertically varying temperature data is not available. The latter incorporates a high degree of physical realism. However, it incurs substantial computational expense as compared to other methods. A third method projects the vertically varying atmospheric temperature to the high-resolution terrain. This is performed by linearly interpolating 3-D atmospheric data to the higher resolution dataset:

$$T_{DS}(i,j) = T_{z_{NAM}}(i,j) + (z_{DEM}(i,j) - z_{NAM}(i,j))\frac{\left(T_k(i,j) - T_{Z_{NAM(i,j)}}\right)}{(z_k(i,j) - z_{NAM}(i,j))},$$

where the subscripts DS, NAM, and DEM correspond to the downscaled variable, model variable, and digital elevation model height, respectively. *i,j* are the zonal and meridional indices of the DEM and *k* is the index representing the nearest model level above the height of the DEM elevation. At DEM grid cells with elevation values *less than* the NWP model terrain, a near surface temperature lapse-rate is determined:

$$\Gamma(i,j) = \frac{(T_1(i,j) - T_0(i,j))}{(z_1(i,j) - z_0(i,j))}$$

The subscripts *0* and *1* indicate the surface and the first model level above the surface. This lapse-rate is then used to *extrapolate* the model and the surface temperature to the height of the DEM grid cell:

$$T_{DS}(i,j) = T_{z_{NAM}}(i,j) - \Gamma(i,j)(z_{DEM}(i,j) - z_{NAM}(i,j))$$

Note that this method requires that the NWP is first interpolated horizontally to the DEM coordinate system. In this framework, an optimal 2-D interpolation scheme is used to interpolate the NAM data from a Lambertian grid to the cylindrical DEM/land cover grid. This 2-D interpolation is non-trivial as the NAM nest model framework uses a spherical Earth projection, and the grid cell center latitude and longitude points are not constant in x/y coordinate space. Therefore, the NAM grid is treated as an unstructured mesh and requires a sophisticated spatial interpolation scheme. For this interpolation, we use the SciPy (Jones et al. 2001), Griddata interpolation

function. This function uses a barycentric triangulation routine to map the unstructured mesh to the DEM. Since the spatial coordinates of the unstructured mesh are constant in time, the interpolation weights are calculated only once at the beginning of the BSHARP initialization. This substantially reduces the computational expense of BSHARP. An example of temperature downscaling is presented in Figure 2.

Figure 2. Example temperature downscaling: Left NAM 3-km Forecast Surface temperature for Feb 18 2020 01 UTC. Right top: Zoomed-in view of 3-km NAM temperature corresponding to the box outlined on the right. Right bottom: NAM 3-km temperature downscaled to the 1-km DEM.

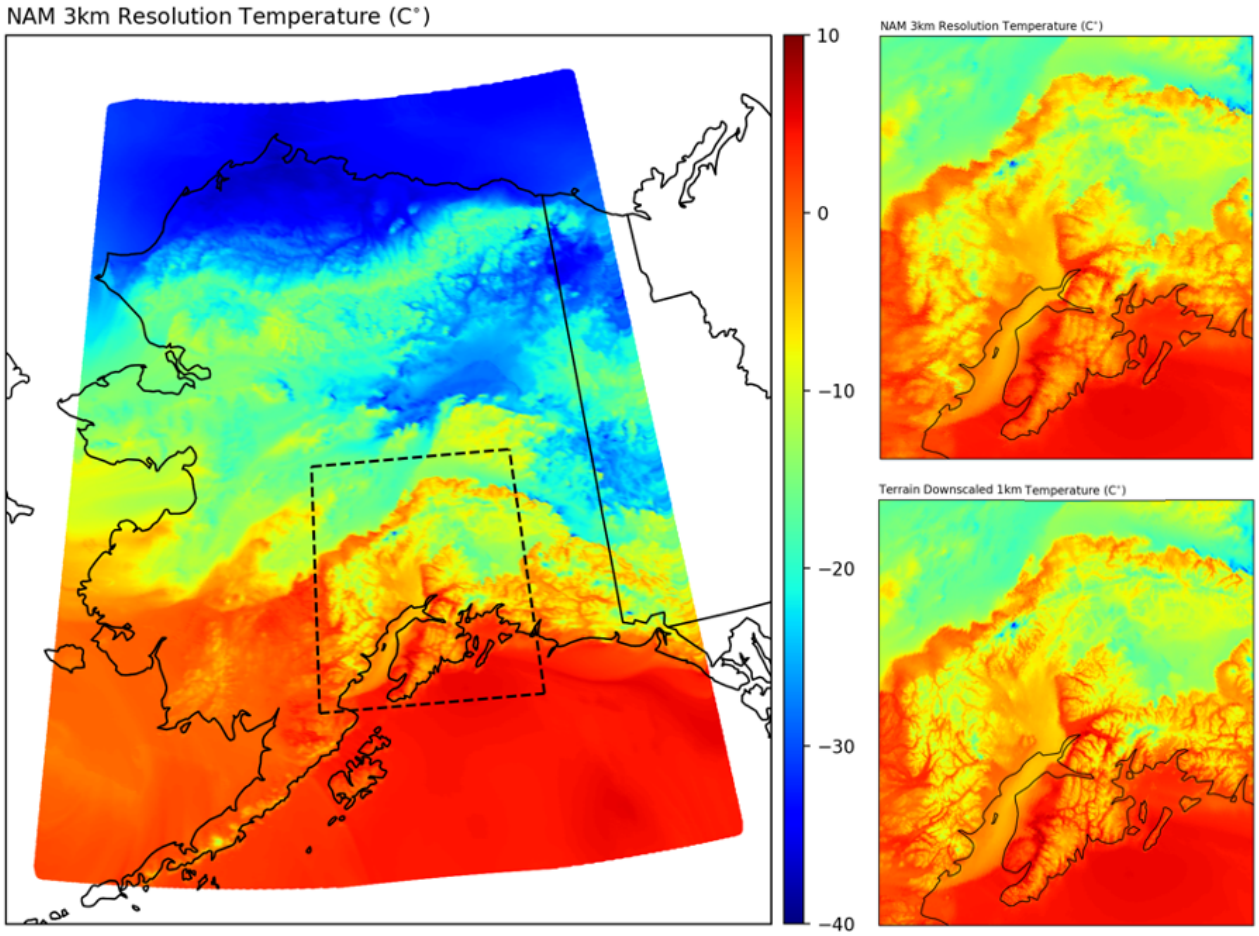

2.2.3 Wind downscaling

The wind-downscaling approach described here is similar to the approach for temperature in that the free-atmospheric windspeed is projected onto the DEM terrain. Note that during the wind-downscaling procedure a check is performed to replace any down-scaled wind values less than 0.1 to

0.1 m s^{-1} to maintain physical realism. The wind is then adjusted for the effects of an overhead forest canopy (e.g., Liston and Elder 2006; Belcher et al. 2012):

$$V_c = Ve^{-0.9LAI\left(1-\frac{z}{h_{veg}}\right)},$$

where h_{veg} is the canopy height, z is some reference height within the canopy (assumed $z=0.6h_{veg}$), and LAI is the leaf-area-index, a variable that quantifies the overhead fraction of the canopy foliage. Note that in adjusting the windspeed for the canopy, the windspeed reference height is modified from the NAM output 10 m to 0.6 h_{veg} following Liston and Elder (2006). An example of the downscaled wind is presented in Figure 3.

Figure 3. Example wind speed downscaling: Left NAM 3-km Forecast 10-m wind speed for Feb 18 2020 01 UTC. Right top: Zoomed in view of 3-km NAM wind speed corresponding to the box outlined on the right. Right bottom: NAM 3-km wind speed downscaled to the 1-km DEM.

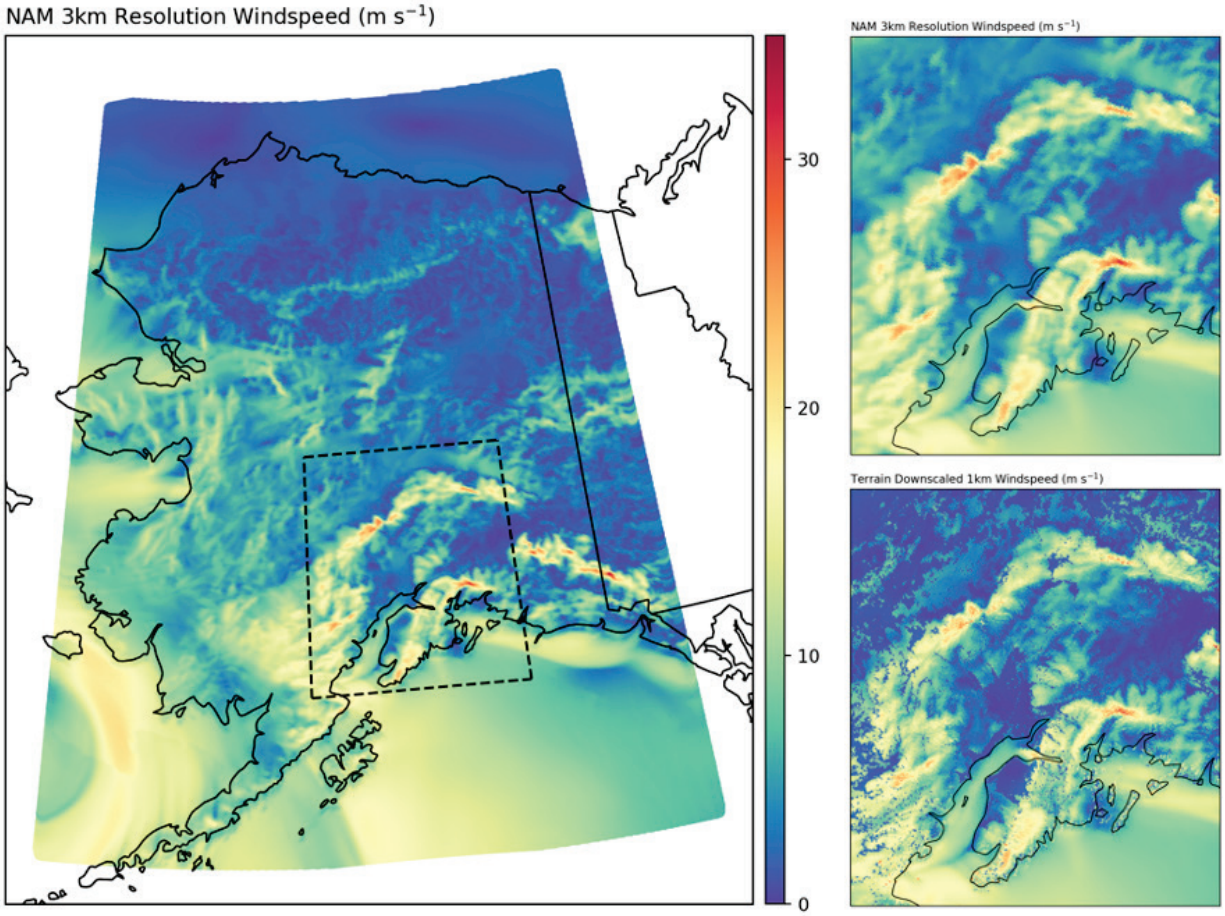

2.2.4 Rain/Snow partitioning

The partitioning between rain and snow is a complicated process that is driven primarily by microphysical processes, atmospheric boundary layer stability and turbulence, and hydrometeor growth trajectories. While many modern NWP models determine the rain/snow partitioning by the microphysics of the atmospheric model, this approach is not universally compatible with the downscaling procedure described here since surface elevation of the DEM can be substantially different than that of the weather model. Instead, we follow the approach of many land surface snow models and partition precipitation into snow and rain as a function of surface temperature. Specifically, we apply the commonly used Jordan (1991) parameterization that partitions rain from snow as a linear function of temperature:

$$f_{snow} = \begin{cases} 0, & T_{sfc} > 2.5\ °C \\ 0.6, & 2.0 < T_s \leq 2.5\ °C \\ 1 - (-54.623 + 0.2T_s), & 0.5 < T_s \leq 2.0\ °C' \\ 1., & T_s \leq 0.5°C \end{cases}$$

where f_{snow} is the fraction of precipitation determined to be snow.

The downscaled new snow is primarily used for refreshing the surface snow characteristics and determining the amount of snow available for lofting.

For the prediction of blowing snow, the above parameterization is likely sufficient in most instances since snow bonding increases (and erodibility decreases) as the temperature approaches freezing, and therefore as the temperature enters into the mixed-phase regime, the possibility for mis-identification of snow or rain likely has minimal impacts on the blowing-snow risk. In other words, once it's warm enough for mixed precipitation, blowing snow is unlikely to occur, regardless of the wind speed. An exception to this would be in cases of sleet or freezing rain-events, which occur due to the presence of a shallow cold layer near the surface underlying a warm (above freezing) layer aloft. While these events usually occur when the temperature is just below freezing, they can occur at surface temperatures as low as -10 °C (Cortinas et al. 2004). While we acknowledge that these events may be a detriment to blowing-snow prediction, we expect that they are rare and have only a minor impact.

2.3 Surface snow characteristics and erodibility

While the Noah LSM contains a basic energy and mass balance snow model, it is relatively simplistic compared to a majority of currently available snow models.

Fundamental to blowing-snow prediction is the character and quality of the snow exposed to mechanical lofting. Fresh snow essentially refreshes the surface snow, and therefore understanding the character of fresh snow is essential towards accurately predicting blowing-snow risk. The character of snow is often described in qualitative terminology; for example, is the snow light and fluffy vs. heavy and dense? Is it made up of fragile dendrites or rimed needles? These qualities have a large impact on how erodible fresh snow is, and therefore they need to be described quantitively. The Crocus snow model (Brun et al. 1992; Vionnet et al. 2012) contains an advanced parameterization for snow character that is adapted to generate a diagnostic threshold wind speed for BSHARP.

Crocus has a three-variable quantitative snow character parameterization that evolves in time as a function of snow temperature and liquid water content (dry-metamorphosis and snow melt) and wind (wind packing). Crocus snow character is determined by dendricity (d), sphericity (s), and grain-size (g_s). These variables are initial values as functions of near-surface wind speed following:

$$d_0 = \begin{cases} 0.2, V \geq 6.14 \\ 1.29 - 0.17V, 1.70 \leq V < 6.14 \\ 1.0, V < 1.70 \end{cases}$$

$$s_0 = \begin{cases} 0.5, V < 1.5 \\ 0.38 + 0.08V, 1.5 \leq V < 6.5 \\ 0.9, V \geq 6.5 \end{cases}$$

Initial snow is given a constant grain-diameter for all atmospheric conditions (~0.3 mm).

These variables then evolve in time as a function of the temperature gradient and liquid water content of the snowpack. The specific functions for this evolution are described in detail in Vionnet et al. (2012). A qualitative schematic of how a snow grain transitions from a dendritic state to a spherical or non-spherical state and how it grows in time under different snowpack temperature gradient regimes is presented in Figure 4.

In the dry growth (i.e., no liquid in the snowpack) snow grain dendricity decreases until it is 0, and sphericity either increases or decreases depending on the temperature gradient of the snowpack. Once d=0, the snow grains are considered either spherical or non-spherical (s=0). Non-spherical snow grains then increase in size over time under "strong" temperature gradients ($dT/dz>5$ K m^{-1}), simulating the growth of depth hoar. Under weak gradients, non-spherical snow grains can regain their sphericity. Critically, while undergoing dry metamorphosis, spherical snow grains do not change in size, and while snow grains can transition back and forth between spherical and non-spherical, they can never regain dendricity.

Figure 4. Schematic of the dry growth regime for snow grains in Crocus. Circles indicate spherical snow, and hexagons indicate non-spherical snow (i.e., faceted snow grains). SG = Strong Gradient, WG = Weak Gradient.

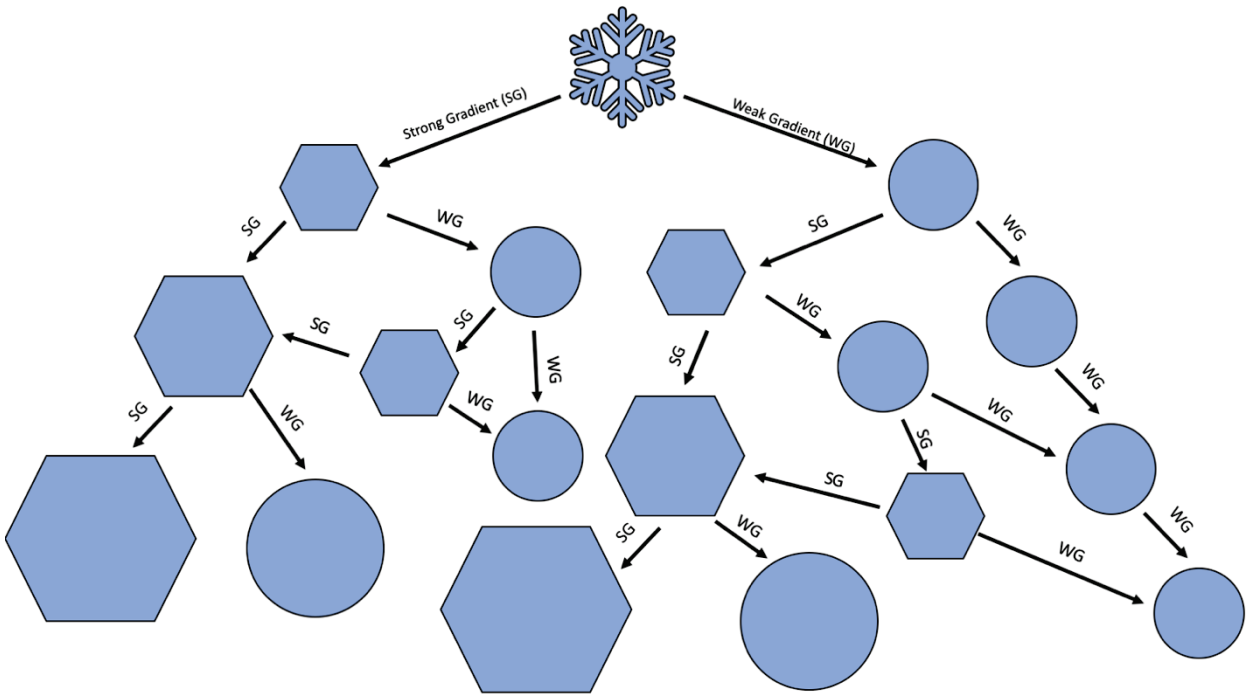

Under wet-growth (LWC>0), d rapidly approaches zero, and large spheroid grain clusters develop.

Due to the relatively simple treatment of snow in the Noah LSM, in particular the combined single layer snow/soil surface model, the application of the Crocus dry-metamorphosis snow aging parameterization is complicated since it relies on a snow temperature gradient. To approximate a temperature gradient from the NAM, we use

an approach that relies only on the downscaled 2m temperature and simulated snow depth. The reliance on 2-m temperature is chosen to accommodate the downscaling procedure without requiring the use of a full surface energy balance model.

In reality, snow is well-approximated as a continuous medium through which heat transfer is a diffusive process scaled by a thermal conductivity determined by the snowpack properties (Sturm et al. 1997). As a result, snow acts as a natural, low-pass filter of atmospheric surface temperature with a damped downward propagation of surface temperature variability through the snowpack with time.

In the approach here, we aim to replicate this behavior in a simple manner as a means of approximating a near surface snowpack temperature gradient. To accomplish this, the snowpack temperature at depth (z) is computed as a weighted mean between the downscaled 2-m temperature, and the snowpack temperature at z from the previous timestep:

$$T(t,z) = W(z)T(t-1,z) + \big(1 - W(z)\big)T_{2m}(t),$$

where the weights ($W(z)$) are determined as a function of snow depth such that the temperature is more heavily weighted towards its previous value at deeper snow depths:

$$W(z) = 1.0 - 0.5e^{\frac{-z}{8}}\Delta t,$$

where $W(z)$ is the weight at height z (in centimeters), and Δt is the timestep in hours. This parameterization generates thermal profiles that are, to first-order, representative of commonly observed snow packs (e.g., Fierz 2011). To illustrate this approximation, the parameterized snowpack temperature profile is presented at 4 times for a 0.7-m-deep snowpack forced with a sinusoidal 2m temperature with an amplitude of 10 K representing one full diurnal temperature cycle (Figure 5).

Figure 5. Idealized temperature profiles used to approximate a near surface temperature gradient (TG) in BSHARP for 4 different times forced with an idealized 2m temperature diurnal cycle. Markers indicate the temperature at 8% of the snowpack depth, i.e., the bottom boundary for computing the near surface temperature gradient. Note that the near surface temperature gradient (TG) used to compute dry-metamorphosis is the temperature gradient between the markers and the surface.

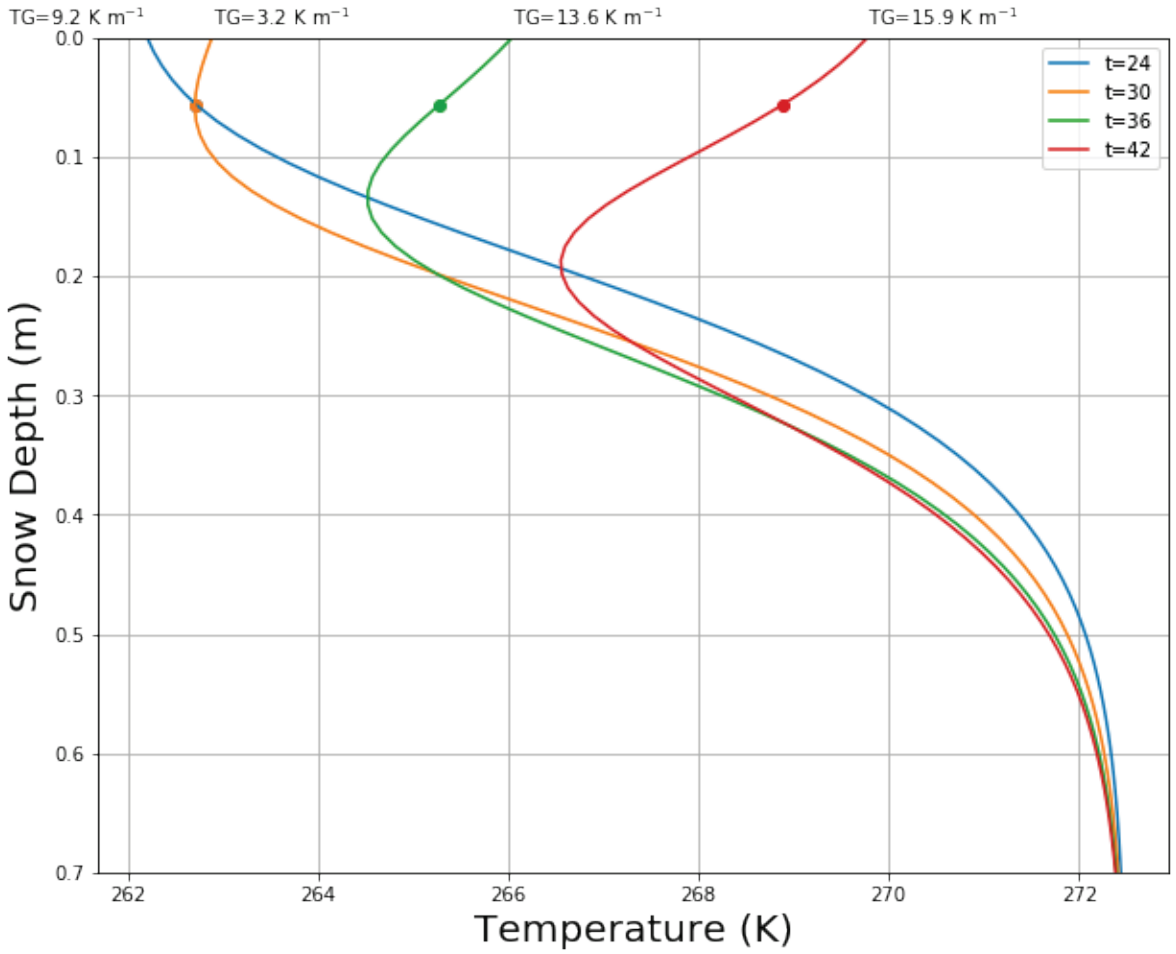

We note that while this approximation introduces both memory and a downward propagating temperature signal that is a good first order representation of observed snowpacks, it may be a poor approximation for snowpacks subject to rapid, large variations in 2-m temperature and for thinner snowpacks. We acknowledge that the above approximation is a simplification made to accommodate the forcing dataset and downscaling procedure described in sections 2.1 and 2.2 and that a more sophisticated treatment of the snowpack would almost certainly yield more accurate results. However, we argue that in this specific context, errors in the

above approximation are not likely to have a dominant influence on the u_{*t} or blowing snow risk predictions.

Not only do dendricity, sphericity, and density evolve as a function of temperature, they change in response to the wind if the wind speed exceeds the threshold wind speed determined from an empirically derived "mobility index" (m_o) determined from d, s, g_s, and ρ_s. This simulates mechanical destruction of snowflakes and snow surface packing due to collisions that occur during snow drifting (i.e., wind-packing). We refer the reader to Vionnet et al. (2012) for the specific wind-packing function.

The threshold windspeed in Crocus is the quantitative metric of snow erodibility and is as follows. First, the snow mobility index as determined by the snow surface characteristics:

$$m_0 = \begin{cases} 0.34(0.75d - 0.5s + 0.5) + 0.66F(\rho_s), d > 0 \\ 0.34(-0.58g_s - 0.833s + 0.833) + 0.66F(\rho_s), d = 0' \end{cases}$$

where $F(\rho_s)$ is a function of the surface snow density (in kg m^{-3}):

$$F(\rho_s) = [1.25 - 0.0042(\max(\rho_s, 50) - 50)]$$

The mobility index is then used to compute a "driftability index" (S_I) dependent on the 5 m windspeed (V):

$$S_I = -2.868e^{-0.085V} + 1 + m_0$$

When $S_I \leq 0$, then the windspeed is insufficient to sustain snow drifting and, thus, the threshold windspeed (U_t) is attained by setting S_I=0 and solving for V:

$$U_t = \ln\left(\frac{1 + m_o}{2.868}\right)\frac{1}{0.085}$$

Note that in Crocus, the rates of change in snow properties due to wind-packing are proportional to S_I.

Notably, as dendricity decreases and sphericity increases, the mobility index decreases and the threshold windspeed increases, indicating that as snow grains evolve from dendritic to spherical, they become less mobile. Similarly, as snowpack density and particle grain size increase, the snow

surface also becomes less erodible, which is generally in accordance with observations in nature.

While empirical, the above functions represent numerous relevant physical processes related to snow surface erodibility including wind compaction, snow grain evolution, the impact of wet snow, and the effects of snow particle shape. This makes the Crocus snow aging parameterization an attractive choice for BSHARP. However, we note a distinct lack of a temperature dependency in the parameterization indicating that the temperature effect on interparticle bonding strength (i.e., sintering) is not incorporated into the Crocus framework and is a key missing process.

One considerable downside of the Crocus parameterization is that its component variables (i.e., dendricity, sphericity) are not physically measurable and are practically impossible to evaluate using standard observations. However, the net output of this framework has been well-validated using observations collected in the French Alps and can provide significant aid in differentiating where snow is most erodible from where it is not erodible (e.g., Vionnet et al. 2013).

In BSHARP, snow erodibility is cast in terms of U_t using the thresholds in Table 1:

Table 1. Thresholds used to qualitatively designate snow erodibility.

Qualitative erodibility description	U_t value
Highly Erodible (red)	$U_{t,5} \leq 6.5 m\ s^{-1}$
Somewhat Erodible (yellow)	$6.5\ m\ s^{-1} < U_{t,5} \leq 11.5\ m\ s^{-1}$
Not Erodible (light green)	$U_{t,5} > 11.5\ m\ s^{-1}$
Not Snow Covered (dark green)	$U_{t,5} > 27.5\ m\ s^{-1}$

2.4 Tier 2: Probabilistic blowing snow

The simplest approach to forecasting the possibility of blowing snow at any given grid cell within the domain using this framework is to difference the 5-m windspeed and the 5-m threshold windspeed and assume blowing snow is possible anywhere this difference is greater than zero. However, this binary ("yes/no") forecast technique can be complicated due to errors in the wind forecast, threshold wind speed, and wind gustiness. We therefore argue that a probabilistic approach for assessing the blowing snow risk is more valuable to the end user than a simple binary mask.

To estimate a "probability" of blowing snow, a Rayleigh distribution is constructed as a wind speed probability distribution function for each grid cell. We chose a Rayleigh distribution as climatological windspeeds can be reasonably well-described by this kind of distribution (e.g., Justus et al. 1978; Tuller and Brett 1985). The Rayleigh distribution is then integrated over the windspeeds that exceed the threshold windspeed to compute a probability of blowing snow. The distribution is scaled such that the majority of the data falls within ± 1.25 m/s of the model output wind in efforts to account for unpredictable wind errors as well as sub-spatial and sub-temporal variability. An idealized illustration of this probabilistic approach is presented in Figure 6.

Figure 6. Idealized Rayleigh distribution of windspeed centered at 4.45 m/s with a threshold wind speed at 5.2 m/s. Under this scenario, there is an 18% probability of the windspeed exceeding the threshold, indicating that this situation would be classified as "blowing snow unlikely." Green shading shows the integrated distribution where the wind exceeds the threshold.

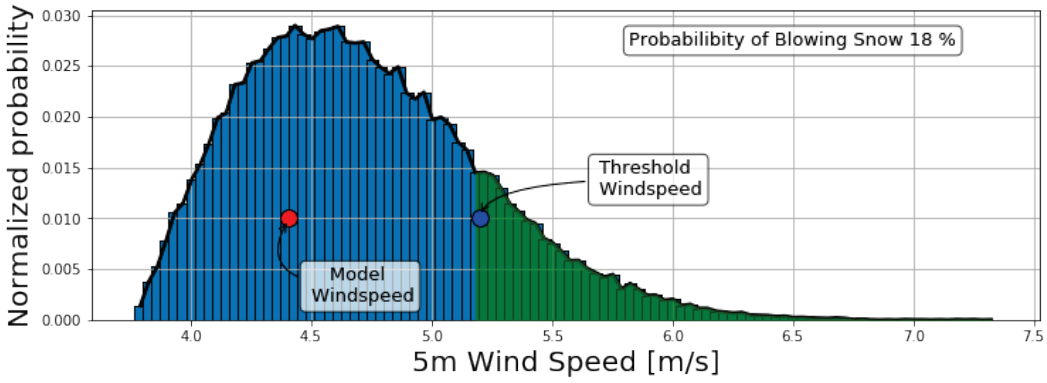

We note that the probabilistic approach here is not based on any observational data and is not meant to be used as a robust quantitative metric. Rather, it is designed as a qualitative aid towards differentiating grid cells where the difference between U_t and U is sufficiently small such that marginal deviations in the wind forecast or uncertainties in snow erodibility are likely to change whether or not U_t is likely to exceeded by the wind. This approach will better aid in decision planning activities than a simple binary product, which is more sensitive to irreducible uncertainty and sub-grid wind speed variability. A qualitative assessment of probability is given using the thresholds in Table 2:

Table 2. Thresholds used to give qualitative assessment of probability.

Qualitative Probability Description	Probability Threshold
Blowing snow unlikely or snow cover = 0 (green)	$P \leq 20\%$ and/or $SCA = 0$
Blowing snow possible (yellow)	$20\% < P \leq 85\%$
Blowing snow likely (red)	$P > 85\%$

2.5 Tier 3: Deterministic blowing snow visibility forecast

2.5.1 Saltation and turbulent suspension

Like soils, the blowing snow saltation process is parameterized as a function of the difference between the applied wind stress and the threshold wind stress. Following the derivation of snow saltation presented in Pomeroy and Gray (1990), which is based on principles first described in Bagnold (1941), the transport rate of saltating snow is:

$$Q_{salt} = \frac{u_p E(\tau - \tau_n - \tau_t)}{g},$$

where u_p is the mean particle velocity, E is a non-dimensional saltation efficiency coefficient between 0 and 1 and g is the gravitational constant. τ is the atmospheric shear stress and is a function of the friction velocity and atmospheric air density:

$$\tau = u^{*2}\rho_{air}.$$

τ_n is the non-erodible stress and assumed to be zero over conditions with complete snow cover. τ_t is the stress applied to the erodible fraction. Pomeroy and Gray (1990) contend that the particle velocity (u_p) can be expressed as a function of the threshold friction velocity:

$$u_p = cu_t^*,$$

where c is a proportionality constant. Combining the above equations yields:

$$Q_{salt} = \frac{cu_t^* E\rho_{air}}{g}(u^{*2} - u_t^{*2}).$$

This is similar to saltation flux equation for soils with one critical difference: Q_{salt} is proportional to u^{*2} instead of u^{*3}. Pomeroy and Gray (1990) attribute this difference to their formulation showing that saltation velocity is a function of u_t^* and not u^*. Furthermore, Pomeroy and Gray (1990) propose that the saltation efficiency constant (E) is inversely proportional to u*, analogous to the concept of kinetic friction. Finally, Pomeroy and Gray (1990) combine the c and E constants into an empirically fitted parameter to express the saltation flux as:

$$Q_{salt} = \frac{0.68}{u^*}\frac{u_t^*\rho_{air}}{g}(u^{*2} - u_t^{*2})$$

We choose the above formula for the saltation model used in BSHARP. It is chosen for its simplicity and also for its $1/u^*$ multiplier. The $1/u^*$ multiplier better differentiates this function from that of saltation functions designed for soil, and it has been speculated upon in the literature that this multiplier is unique to blowing snow saltation and is related to particle fracturing at the surface (which generates the small particles that enter turbulent suspension) (e.g., Pomeroy and Gray 1990).

To use the above formulation for Q_{salt}, the threshold wind velocity (U_t) is first converted to a static threshold surface friction velocity. Typically, a log-profile is used to estimate the wind at height (z) above the surface as determined by the surface roughness length. In the simple case, where atmospheric stability corrections are not applied, this relationship is used to relate surface friction velocity to windspeed as follows:

$$u^* = U_z\frac{\kappa}{\ln\left(\frac{z}{z_0}\right)},$$

where κ is Von-Karmen's constant (equal to 0.4), and z_0 is the surface roughness length for momentum (i.e., the height above the ground at which the wind ceases). For snow surfaces, the roughness length is usually accepted to be somewhere between 0.001 and 0.004 m. The threshold surface friction velocity (u_t^*) is given by plugging U_t into the above equation with z = 5 m. Neutral atmospheric stability is assumed for simplicity.

Similarly, u^* is computed from the downscaled 10-m wind using the same formulation with the same neutral stability assumption. However, for a

snow surface that is actively saltating, particle drag within the surface layer retards the windspeed near the surface and effectively increases the roughness length. Therefore, when computing u^* from the 10 m, u^* and z_o are considered coupled and are solved using an iterative approach similar to the method described in Liston and Sturm (1998):

$$z_o = \frac{0.12u^{*2}}{2g}$$

Once a saltation flux is computed, a reference height concentration is estimated from the saltation flux. For determining the reference height, we use the form presented in Pomeroy and Gray (1990) for consistency with the saltation formula.

$$h_r = 1.6\frac{u^{*2}}{2g}$$

From h_r, a reference blowing snow concentration is computed from the saltation flux (Q_{salt}), the friction velocity (u^*) and the reference height (h_r):

$$q_{b,r} = \frac{Q_{salt}}{u_p}\frac{0.45g}{u^{*2}}e^{-0.45\frac{h_{salt}g}{u^{*2}}}.$$

This function is presented in Vionnet et al. (2014) and is part of the Crocus blowing snow model framework. We chose this function for the $q_{b,r}$ because it has a strong physical basis and is almost certainly more realistic than simpler functions that assume the blowing snow concentration is constant with height throughout the saltation layer.

To estimate a blowing snow concentration at 2 m above ground, we use the function described in Pomeroy et al. (1993). This function is advantageous from a numerical modeling perspective in that it's a simple steady state approximation that reduces to a simple exponential decay function based on the reference concentration and friction velocity:

$$q_{b,z} = q_{b,r}exp[-1.55(0.05628u^*)^{0.544} - z^{-0.544}]$$

Due to the steady state assumption in the above formula, it is unnecessary to explicitly compute a sublimation effect on the

concentration at height z, since it is likely already implicit in the above empirical formula. Furthermore, benchmark computations made with the above formula produce more reasonable blowing snow concentrations at 2 m above ground than the relationship described in Kind (1992) and adapted in Liston and Sturm (1998).

We note that fetch is an important factor not included in the diagnostic blowing snow saltation function. We chose to neglect fetch in this framework due to the 1km scale of the grid. According to Liston and Sturm (1998) fetch has the largest scaling influence on Q_s at the sub 500m scale and would have little influence if implemented on the 1-km grid spacing. However, as BSHARP is refined to finer resolution grids, fetch should be considered.

2.5.2 Visibility

Following the above frameworks for $q_b(z)$ blowing impacts on visibility are introduced following the framework laid out in Pomeroy and Male (1988). In their study, they combine a gamma-size distribution with Mie scattering theory and the Koschmieder relationship (e.g., Horvath 1971) to compute atmospheric visibility as a function of blowing snow mixing ratio:

$$Vis = \frac{5.217\bar{r}\rho_p}{\rho_d \overline{Q_{EXT}} c_\alpha},$$

where $\bar{r}$ is the mean particle radius (m) and ρ_p is the particle density (assumed to be near that of pure ice: 900 kg m^{-3}). Q_{EXT} is the mean extinction coefficient, c_α is the gamma-function shape correction factor, and ρ_d is the particle drift density (i.e., q_b). While the relevant supporting formulas for Q_{EXT}, $\bar{r}$, are c_α are presented here, the full derivation described in Pomeroy and Male (1988) is not provided.

The gamma shape correction factor (c_α) is given as:

$$c_\alpha = \frac{(\alpha+1)!\,\alpha}{(\alpha+2)!},$$

where α is assumed to be between 2 and 15 (e.g., Dery and Yau [1999] and Pomeroy and Male [1988]).

$\bar{r}$ relies on a several assumptions regarding the particle number concentration and tuning parameters (e.g., Dery and Yau [1999]). For

simplicity, a particle radius of 50μm and an $\alpha = 10$ are assigned, as these values showed the best agreement in for observations of Antarctic blowing snow (Huang et al. 2008). Q_{EXT} is given by:

$$\overline{Q_{EXT}} = 1.82\bar{r}^{-0.011}$$

By merging the preceding formulas, a function for visibility as it relates to blowing-snow mixing ratio is written as:

$$Vis = \frac{5.217\bar{r}\rho_p}{1.82q_{b,z} * \bar{r}^{-0.011}c_\alpha},$$

Note, that because of the size of blowing snow particles the Mie scattering approximation holds throughout the visible and infrared spectra, and thus the above formulation works well throughout this spectral range (Pomeroy and Male 1988).

In BSHARP, blowing-snow visibility is cast as a deterministic variable with the units of kilometers. Note, that this visibility forecast accounts only for blowing snow hydrometeors and no other visibility reducing particles (e.g., snow or rain precipitation and fog). The above framework for estimating blowing snow saltation, concentration, and visibility performed remarkably well for a case-study simulation for a well-observed blowing-snow event in the North Central United States (Letcher et al. 2020: submitted WAF).

2.6 Model implementation and output format

In this report, BSHARP is run in "forecast" mode forced with operational NWP data from the NAM as a demonstration. Each forecast is run out to 48 hr past model initialization, and the data is output to NetCDF format on a 1-hourly frequency. Since the snow aging process extends well past 48 hr, the BSHARP simulated snow surface state (i.e., d, s, g_s, ρ_s) is saved every 24-hr output time and is used to initialize the snow state of the next model run. This process is illustrated graphically in Figure 7.

Figure 7. Flow chart graphic depicting the model forecast procedure with forecast time oriented top-to-bottom vertically, and model integrations left-to-right horizontally.

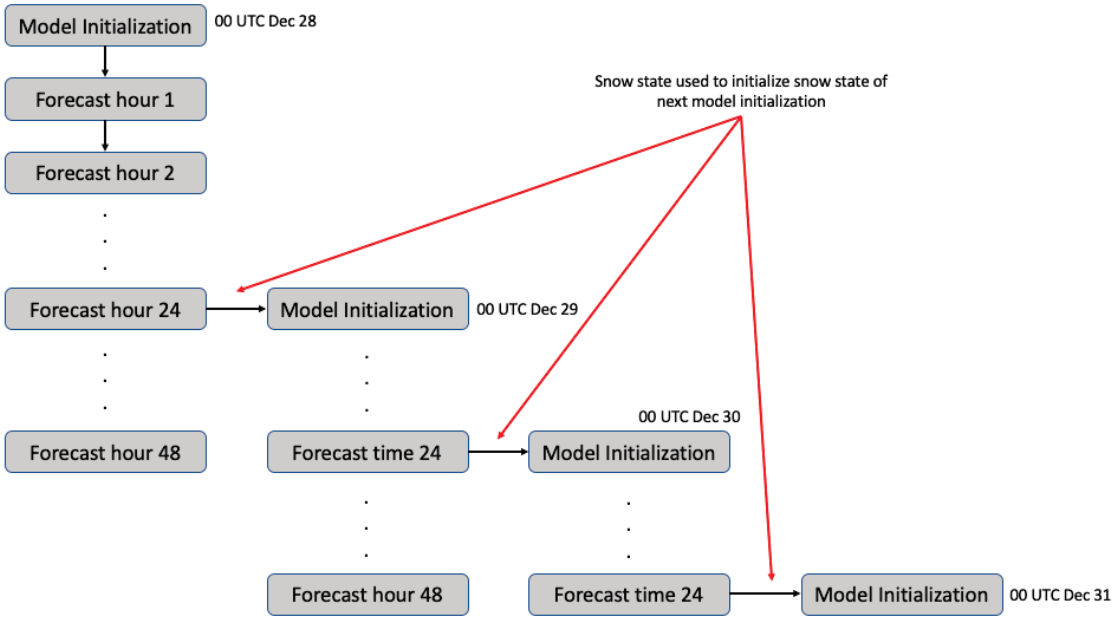

The tiered output levels can be saved to time-stamped Geotiff format for any timestep for compatibility with GIS software and map-based planning services.

3 Demonstration

We demonstrate the BSHARP tiered risk assessment by showing snapshot examples of erodibility risk (Figure 8), forecast blowing snow probability (Figure 9), and forecast blowing snow visibility (Figure 10) for selected times that occurred throughout the winter 2019-2020 season in Alaska.

Figure 8. Simulated erodibility Risk from BSHARP. Risk is valid for times indicated on figure.

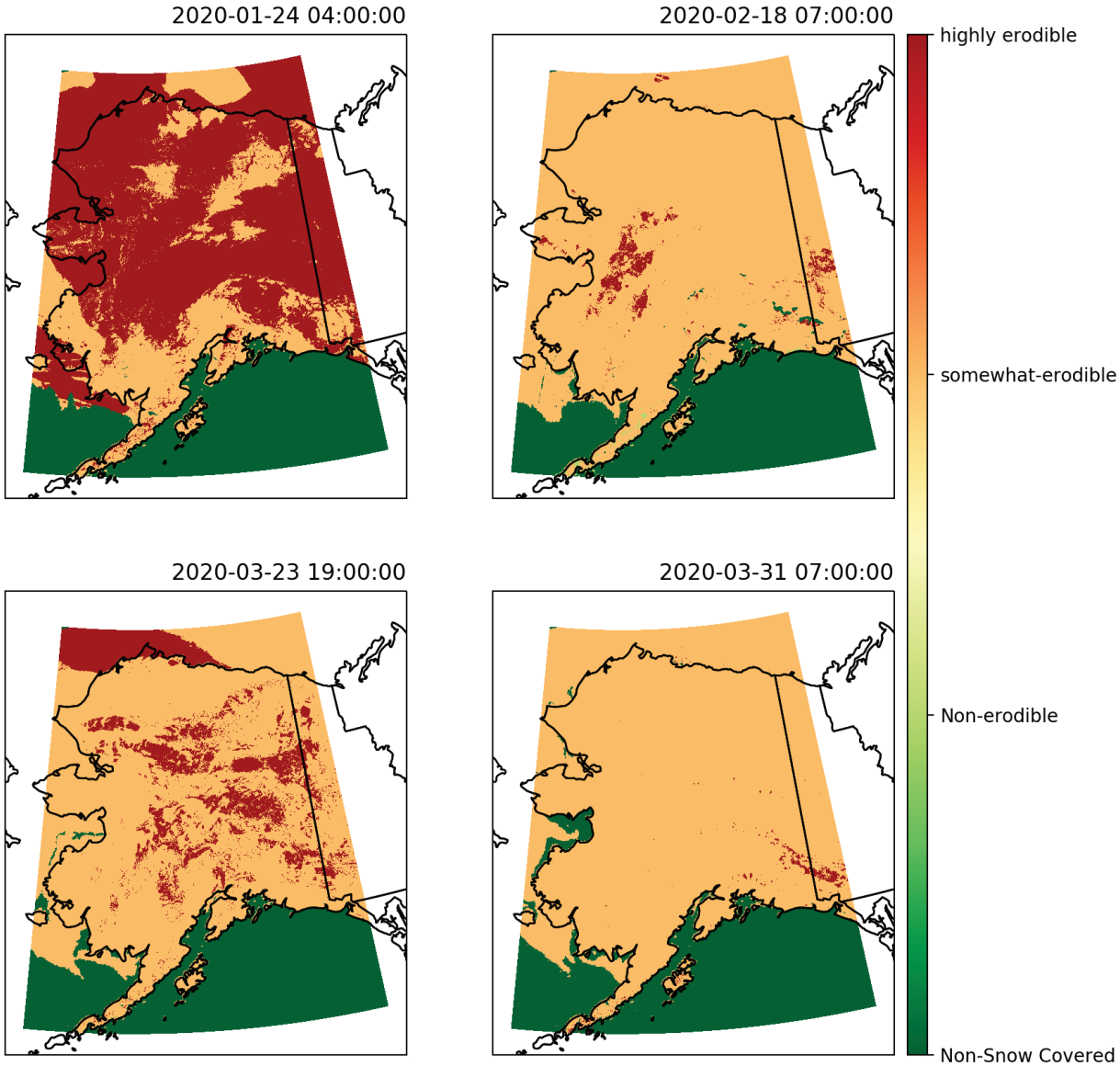

Figure 9. Simulated probability of blowing snow for 4 different times within the 2019-2020 winter season. Markers show where automated weather observing stations reported blowing snow within the 12-hr time period surrounding the output time, color coded from green-to-red based on how many blowing snow reports were recorded during the 12-hr time period.

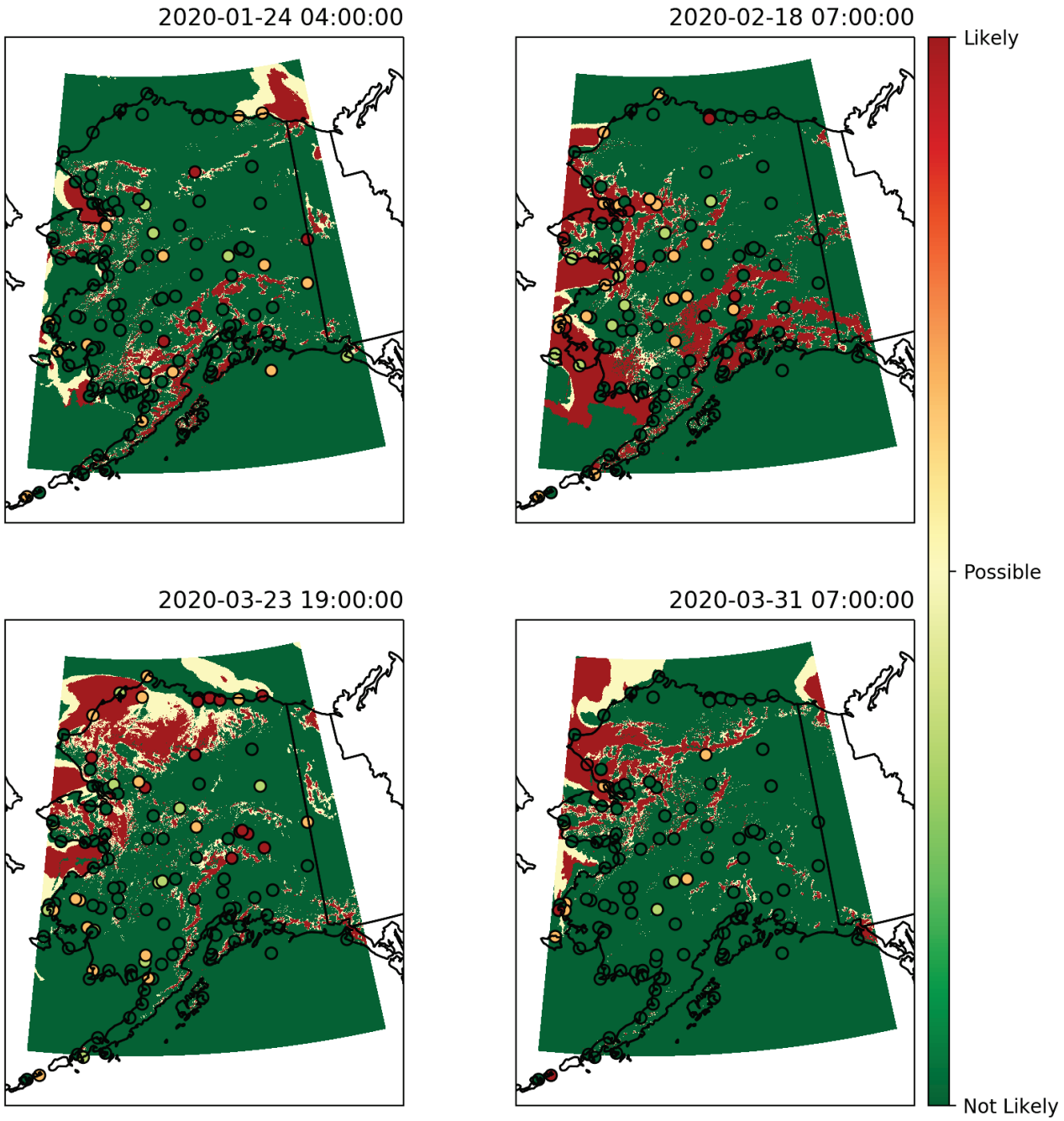

Figure 10. Simulated deterministic blowing snow visibility impacts from BSHARP.

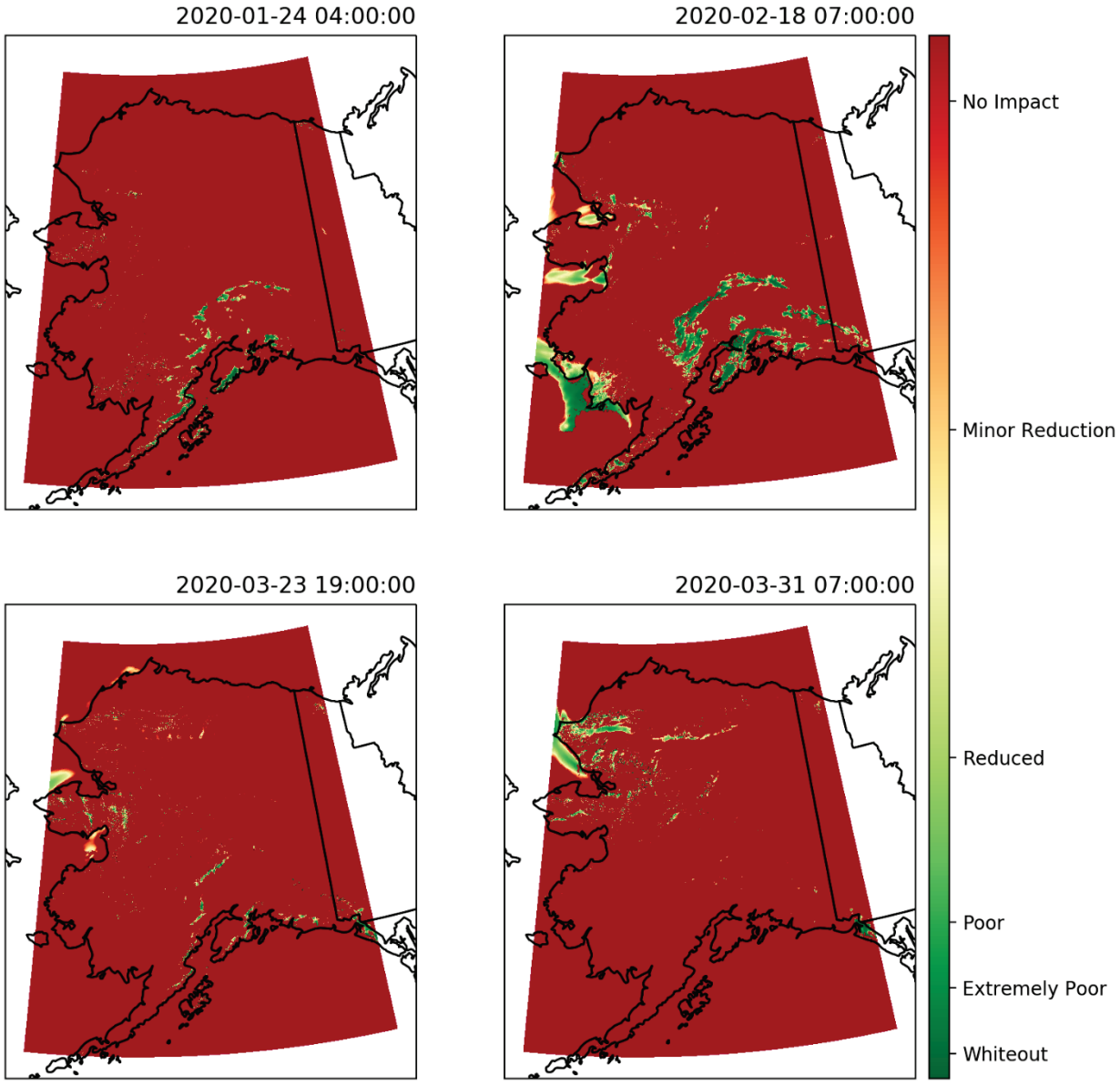

This demonstration of the BSHARP risk assessment illustrates anticipated blowing-snow impacts at high spatial resolution using simple qualitative descriptors. In particular, the high mountains that make up the Alaska and Brooks Ranges are often marked as having a high risk for blowing snow and poor visibility. In many instances, there is a moderate-to-high probability of blowing snow without a coincident visibility degradation, i.e., the Northern Slope for the 23 March 2020 example. This is due to both the comparison of a probabilistic risk assessment to a deterministic visibility forecast, and the fact that exceedance of the threshold friction

speed does not always indicate a visibility reduction at 2 m above ground in the turbulent suspension layer. Furthermore, lateral transport between grid cells in this model is neglected, which leads to the pixelated appearance in the visibility diagnostic.

While we acknowledge substantial uncertainties with the forecast parameters, BSHARP is capable of differentiating times and locations where blowing snow is a likely risk to operations. Note that in the above example images the date stamps and descriptions are generated directly from metadata saved with the Geotiff output files.

4 Software

BSHARP is written in the Python programming language due to Python's accessibility, readability, data I/O packages, and streamlined package and dependency management. There are several non-native package dependencies required to support the various functions of BSHARP:

- Pygrib (required): handles most gridded NWP input data.
- NetCDF4 (required): handles restart file I/O + optional user-output to NetCDF format.
- Matplotlib (required): handles miscellaneous plotting functions
- GDAL (required): handles static DEM input + optional user-output to Geotiff format.
- SciPy (required): handles 2-D optimal interpolation required for downscaling procedure.
- NumPy (required): handles most numerical and array operations including masking.
- Cartopy (optional): can plot geographic data to png files within Python (Met Office, 2010).

Due to the required GRIB I/O support to handle meteorological data stored as GRIB, BSHARP V 1.0 cannot be used on Windows-based platforms as of the time of this publication.

Tests of BSHARP were performed on a Mac-OS with Python version 3.6 managed using the freely available Anaconda package manager. Appendix A provides a simple walkthrough on how to run BSHARP.

5 Conclusions and Recommendations

5.1 Conclusions

This report documents the development and demonstration of the Blowing Snow Hazard Assessment and Risk Prediction model (BSHARP) V 1.0. BSHARP is unique in that it aims to distinguish between erodible and non-erodible snow by using a physically based snow aging parameterization. Furthermore, BSHARP's modular framework allows for fast, moderately complex downscaling of NWP data onto a higher resolution digital elevation model (DEM). Output is stored in a tiered manner in Geotiff format. The test case described here was performed using the NAM Alaska high-resolution nest operational NWP downscaled from its native 3-km resolution to a 1-km DEM and land classification model. BSHARP can improve terrain awareness in extreme conditions and aid in cold regions mission planning by providing a more geographically precise forecast for blowing-snow conditions and impacts.

5.2 Recommendations

While the Crocus snow aging and threshold friction velocity (u_{*t}) parameterizations used in BSHARP have shown promise in helping distinguish from snow covers prone to being mobilized by the wind from snow covers that are not, many gaps remain. For instance, while u_{*t} is a convenient metric for snow erodibility as it is easily adapted into existing saltation parameterizations, it is not a comprehensive parameter. Furthermore, while Crocus has sophisticated snow aging physics, the snow mobility index and subsequently the u_{*t} computation is empirically based and has no direct dependence on snow temperature, which is a key driver of grain bond strength within a snowpack. Finally, the functions estimating turbulent transport from saltation are almost certainly overly simplistic and do not fully represent the processes (including fracture) responsible for generating and lofting small particles that impact visibility. We recommend that future versions of BSHARP can be substantially improved by:

1) Evaluating the snow aging functions used in BSHARP against surface snow micro properties real-world environments.

2) Refining the u_{*t} function to be more physically based.

3) Refining the understanding of how the saltation and turbulent suspension processes are connected over snow using high-speed cameras and image processing software.

4) Coupling BSHARP to a more sophisticated snow model with multiple snow layers to simulate the snow aging process with greater fidelity.

5) Extending the visibility model to incorporate other aspects of visibility degradation. For example, conditions with low-zenith angle overcast on a snow-covered surface in combination with blowing snow.

References

Bagnold, R. A. 1941. *The physics of blown sand and desert dunes*. London: Chapmann and Hall, Methuen.

Benjamin, S. G., J. M. Brown, and T. G. Smirnova. 2016. Explicit precipitation-type diagnosis from a model using a mixed-phase bulk cloud–precipitation microphysics parameterization. *Weather and Forecasting* 31(2):609-619.

Brun, E., P. David, M. Sudul, and G. Brunot. 1992. A numerical model to simulate snow-cover stratigraphy for operational avalanche forecasting. *Journal of Glaciology* 38(128):13-22.

Bychkova, V. I., M. M. Kurbatova, G. A. Zarochentsev, and R. Yu Ignatov. 2018. Blowing snow forecast using numerical atmospheric model output data. *Russian Meteorology and Hydrology* 43(7):444-448.

Cortinas Jr., J. V., B. C. Bernstein, C. C. Robbins, and J. W. Strapp. 2004. An analysis of freezing rain, freezing drizzle, and ice pellets across the United States and Canada: 1976-90. *Weather and Forecasting* 19(2):377-390.

Déry, S. J., and M. K. Yau. 1999. A bulk blowing snow model. *Boundary-Layer Meteorology* 93(2):237-251.

Farr, T. G., P. A. Rosen, E. Caro, R. Crippen, R. Duren, S. Hensley, M. Kobrick, et al. 2007. The shuttle radar topography mission. *Reviews of geophysics* 45(2).

Fierz, C. 2011. Temperature profile of snowpack. In *Encyclopedia of snow, ice and glaciers; Encyclopedia of Earth sciences series*, ed. V. P. Singh, P. Singh, U. K. Haritashya. Dordrecht: Springer.

He, S., and N. Ohara. 2017. A new formula for estimating the threshold wind speed for snow movement. *Journal of Advances in Modeling Earth Systems* 9(7):2514-2525.

Horvath, H. 1971. On the applicability of the Koschmieder visibility formula. *Atmospheric Environment (1967)* 5(3):177-184.

Huang, Q., J. Hanesiak, S. Savelyev, T. Papakyriakou, and P. A. Taylor. 2008. Visibility during blowing snow events over arctic sea ice. *Weather and forecasting* 23(4):741-751.

Ikeda, K., M. Steiner, J. Pinto, and C. Alexander. 2013. Evaluation of cold-season precipitation forecasts generated by the hourly updating High-Resolution Rapid Refresh model. *Weather and Forecasting* 28(4):921-939.

Jordan, R. 1991. *A one-dimensional temperature model for a snow cover: Technical documentation for SNTHERM. 89*. CRREL SR-91-16. Hanover, NH: U. S. Army Cold Regions Research and Engineering Laboratory.

Justus, C. G., W. R. Hargraves, A. Mikhail, and D. Graber. 1978. Methods for estimating wind speed frequency distributions. *Journal of Applied Meteorology* 17(3):350-353.

Kang, L., X. Zhou, T. van Hooff, B. Blocken, and M. Gu. 2018. CFD simulation of snow transport over flat, uniformly rough, open terrain: Impact of physical and computational parameters. *Journal of Wind Engineering and Industrial Aerodynamics* 177:213-226.

Kind, R. J. 1992. One-dimensional aeolian suspension above beds of loose particles—A new concentration-profile equation. *Atmospheric Environment. Part A. General Topics* 26(5):927-931.

Letcher, T. W., S. L. LeGrand, and C. Polashenski. 2021. Applying a physically based blowing snow diagnostic parameterization to improve wintertime visibility forecasts in the WRF model. *Weather and Forecasting* 36(2):615-626.

Li, L., and J. W. Pomeroy. 1997. Estimates of threshold wind speeds for snow transport using meteorological data. *Journal of Applied Meteorology* 36(3):205-213.

Liston, G. E., and M. Sturm. 1998. A snow-transport model for complex terrain. *Journal of Glaciology* 44(148):498-516.

Liston, G. E., R. B. Haehnel, M. Sturm, C. A. Hiemstra, S. Berezovskaya, and R. D. Tabler. 2007. Simulating complex snow distributions in windy environments using SnowTran-3D. *Journal of Glaciology* 53(181):241-256.

Liston, G. E., and K. Elder. 2006. A distributed snow-evolution modeling system (SnowModel). *Journal of Hydrometeorology* 7(6):1259-1276.

Liu, C., K. Ikeda, R. Rasmussen, M. Barlage, A. J. Newman, A. F. Prein, F. Chen, et al. 2016. Continental-scale convection-permitting modeling of the current and future climate of North America. *Climate Dynamics* 49(1-2):71-95.

Minder, J. R., P. W. Mote, and J. D. Lundquist. 2010. Surface temperature lapse rates over complex terrain: Lessons from the Cascade Mountains. *Journal of Geophysical Research: Atmospheres* 115(D14).

Nemoto, M., and K. Nishimura. 2004. Numerical simulation of snow saltation and suspension in a turbulent boundary layer. *Journal of Geophysical Research: Atmospheres* 109(D18).

Pomeroy, J. W., and D. H. Male. 1988. Optical properties of blowing snow. *Journal of Glaciology* 34(116):3-10.

Pomeroy, J. W., and D. M. Gray. 1990. Saltation of snow. *Water Resources Research* 26(7):1583-1594.

Pomeroy, J. W., D. M. Gray, and P. G. Landine. 1993. The prairie blowing snow model: characteristics, validation, operation." *Journal of Hydrology* 144(1-4):165-192.

Schmidt, R. A. 1980. Threshold wind-speeds and elastic impact in snow transport. *Journal of Glaciology* 26(94):453-467.

Steinacker, R., M. Ratheiser, B. Bica, B. Chimani, M. Dorninger, W. Gepp, C. Lotteraner, S. Schneider, and S. Tschannett. 2006. A mesoscale data analysis and downscaling method over complex terrain. *Monthly Weather Review* 134(10):2758-2771.

Tanji, S., and M. Inatsu. 2019. Case study of blowing snow potential diagnosis with dynamical downscaling. *SOLA* 15:32-36.

Tuller, S. E., and A. C. Brett. 1985. The goodness of fit of the Weibull and Rayleigh distributions to the distributions of observed wind speeds in a topographically diverse area. *Journal of Climatology* 5(1):79-94.

Vionnet, V., E. Brun, S. Morin, A. Boone, S. Faroux, P. Le Moigne, E. Martin, and J. M. Willemet. 2012. The detailed snowpack scheme Crocus and its implementation in SURFEX v7.2. *Geoscientific Model Development* 5:773-2012.

Vionnet, V., G. Guyomarc'h, F. Naaim Bouvet, E. Martin, Y. Durand, H. Bellot, C. Bel, and P. Puglièse. 2013. Occurrence of blowing snow events at an alpine site over a 10-year period: observations and modelling. *Advances in Water Resources* 55:53-63.

Vionnet, V., E. Martin, V. Masson, G. Guyomarc'h, F. Naaim Bouvet, A. Prokop, Y. Durand, and C. Lac. 2014. Simulation of wind-induced snow transport and sublimation in alpine terrain using a fully coupled snowpack/atmosphere model. *The Cryosphere* 8:395-415.

Wilby, R. L., T. M. L. Wigley, D. Conway, P. D. Jones, B. C. Hewitson, J. Main, and D. S. Wilks. 1998. Statistical downscaling of general circulation model output: A comparison of methods. *Water Resources Research* 34(11):2995-3008.

Appendix A: Running BSHARP

BSHARP is written in the widely used Python programming language. It is designed to be implemented as a sub-package into a separate Python script through use of the "import" command and called as a stand-alone Python object.

Note that prior to calling the BSHARP python functions, some accompanying Fortran subroutines associated with BSHARP need to be compiled with the "f2py" compiler. These supplementary Fortran subroutines substantially decrease the computational time required to perform the vertical interpolation within the downscaling procedure.

Within a subfolder called "src_ftn" the following command is used to compile the supplementary Fortran code:

```
f2py -m fortran_funcs -c fortran_funcs.f95
```

Once the Fortan code has been compiled, the BSHARP class and code is stored in the sub-folder "main_functions" and can be imported directed into a Python script stored in the parent folder and initialized:

```
from bsharp import main_functions as BSHARP

model=BSHARP.BSHARP(region='alaska',local_path='/path/to/grib/dat
a/',dem_path='/path/to/DEM/tiff/images',restart=True,rst_path='/p
ath/to/restart/netcdf/datafile/')
```

Within BSHARP, there are numerous functions and variables that are called upon to support the main functions within the BSHARP framework. The main BSHARP model class is located within the main_functions library and is accessed as described above. The BSHARP initialization function accepts several optional arguments:

- 'region' – corresponds to a prefix for a DEM and landcover tiff file. In this example, the region is set to 'alaska' and the corresponding tiff file is: "alaska_DEM.tiff"

- 'local_path' – corresponds to the local directory with GRIB2 NWP data is stored.

- 'dem_path' – corresponds to the local directory where the DEM .tiff files are stored

- 'restart' – Boolean flag to indicate whether to try and use a "restart" file to initialize the snow surface state, or start with constant default values.

- 'rst_path' – corresponds to the local directory with restart NetCDF files are located.

- 'lcov' – land cover classification system. Currently BSHARP only accepts the igbp land classification system. Future versions may include other options.

- 'fast_interp' – Boolean flag to turn on fast 2-D interpolation. If true, optimal interpolation weights are generated only on the first time step; otherwise, the full SciPy griddata function is called every time step. The default option is to leave this set to "True" as computing the weights every time step can lead to run times of greater the 1 hr.

During the object initialization, BSHARP performs many initial computational steps, including, for example, loading in the digital elevation model and land cover datasets, computing optimal interpolation weights, and adjusting for the way NAM simulated precipitation data is stored.

Once the object has been initialized, the model is manually integrated through time by the user in a Python script. The model is designed this way due to provide the maximum amount of user control. During the time-integration, each function is called in succession as in the following example. In the following example, BSHARP is used to load and downscale model data at a specific timestep, run the snow history and erodibility parameterization, and compute the blowing-snow diagnostics for 48 time steps (2 days):

```
for t in range(48):

      model.load_model_data(tstep=t) #Loads Meteorological Data
```

```
model.downscale_data() #Downscales data to DEM

model.sfc_snowpack() # Runs the Surface Snowpack aging

model.blowing_snow() # Performs blowing snow diagnostics
```

Note that due to the potentially large memory requirements, the 2-D arrays containing the data are overwritten every time step.

The above example does not save any of the output data; to save the data, the user can call either the "save_to_netcdf" or "save_to_geotiff" function to output data into NetCDF or Geotiff format. Note that with NetCDF format, the user can save multiple variables into one file, whereas with Geotiff, users can save only one variable.

Extending the example for loop described above, to output downscaled temperature, and threshold friction velocity data to a NetCDF file every 6 hr:

```
if (t+1)%6 == 0: #check if a 6 hourly interval

      model.save_to_netcdf(model.ds_var_dict['tmp2m'],'2
meter temperature',’K’,"Downscaled 2 meter
temperature",append=app,fname=’example_netcdf.nc’)

      app = True

      model.save_to_netcdf(model.ds_var_dict['Ustar_thresh'
],'Threshold Friction Velocity’,m/s,"Downscaled threshold
friction velocity",append=app,fname=’example_netcdf.nc’)
```

Note that the model attribute "*ds_var_dict*" indicates the downscaled (*ds*) variable. The raw NAM output can be accessed through "*var_dict*." The "*save_to_netcdf*" function accepts four required arguments in the following order:

1. 2-D array containing output data with dimensions matching the downscaled lat/lon coordinate system

2. NetCDF variable output name

3. NetCDF variable units

4. NetCDF variable description (long name)

Additional arguments include “app”, which is a Boolean flag that indicates whether or not to append the data to the NetCDF file or create a new file. In this example, app is set equal to “True” after the first instance, such that each subsequent time step, data is appended to the NetCDF file. Finally, the file output path is set using the “fname” argument.

To demonstrate the “*save_to_geotiff*” function, the above example is extended to include saving a probability of blowing snow to a Geotiff:

```
strptime=datetime.datetime.strptime(str(model.var_dict['val
idTime']),'%Y-%m-%d %H:%M:%S')

timepfx=strptime.strftime('%Y%m%d%H') ## prefix for file
name.

model.save_to_raster(model.ds_var_dict['Prob_of_blowing'],f
name='ProbOfBlowing_%s.tiff'%timepfx)
```

Note, that in this example the Python datetime package is used to extract the model forecast hour from the BSHARP object and use it to set the filename for the Geotiff file.

A summary function that generates three output Geotiff files following the tiered risk assessment described in section two can also be called using the “*save_geotiffs*” function. The save_geotiffs function automatically datestamps each output file name. It takes up to two optional arguments where a user can modify the threshold values that delineate the different threat levels.

1. ust_thresh (default = [0.31,0.6,1.4])

2. probthresh (default = [20,60])

The function will save three Geotiff files with the prefixes “erod,” “prob,” and “vis” corresponding to the erodibility assessment, blowing-snow risk, and deterministic blowing-snow visibility forecast. Following the example:

```
model.save_geotiffs()
```

Finally, restart files can also be saved by calling a the “save_restart” function within the model class:

```
model.save_restart()
```

This function will save the necessary snow surface information to initialize the snow surface at the beginning of a new simulation. For example, when the next NWP model run becomes available.

Appendix B: Obtaining and Subsetting the DEM and Land Cover Datasets

To use the downscaling procedure within BSHARP a digital elevation model (DEM) and land cover dataset matching the IGBP land classification system.

Publicly available datasets from the USGS are accessible through the USGS "Earth Explorer" website: https://earthexplorer.usgs.gov.

Alternatively, users can use their own DEM and land-cover dataset as long as it is input into the model as a geotiff file using a lat/lon coordinate system.

Once a DEM and landcover dataset are identified in Geotiff format, Gdal can be used to subset the data from the command line. For example, the subset DEM and landcover datasets here were created typing the following commands into the command line:

```
gdal_translate -projwin -167 55 -138 72 nademl_ll.tif
alaska_dem_ll.tif

gdal_translate -projwin -167 55 -138 72 naigbpl20_ll.tif
alaska_igpb_ll.tif
```

Note that in order for this to work, Gdal must be installed on one's machine. Gdal translate is accessible as long as Gdal has been installed using a Python package manager.

Acronyms and Abbreviations

AFWA	Air Force Weather Agency
AGL	Above Ground Level
BSHARP	Blowing Snow Hazard Assessment and Risk Prediction
DEM	Digital Elevation Model
GIS	Geographic Information Systems
GRIB	GRIdded Binary
LAI	Leaf Area Index
LSM	Land Surface Model
LWC	Liquid Water Content
NAM	North American Mesoscale Model
NDAS	NAM Data Assimilation System
NDFD	National Digital Forecast Database
NMM	Non-hydrostatic Mesoscale Model
NOAA	National Oceanic and Atmospheric Administration
NORCOM	North Combatant Command
NSIDC	National Snow and Ice Data Center
NWP	Numerical Weather Prediction
RRTM	Rapid Radiative Transfer Model
SRTM	Shuttle Radar Topography Mission

SWE	Snow Water Equivalent
UTC	Universal Time Coordinate
WRF	Weather Research and Forecast Model

REPORT DOCUMENTATION PAGE

Form Approved
OMB No. 0704-0188

Public reporting burden for this collection of information is estimated to average 1 hour per response, including the time for reviewing instructions, searching existing data sources, gathering and maintaining the data needed, and completing and reviewing this collection of information. Send comments regarding this burden estimate or any other aspect of this collection of information, including suggestions for reducing this burden to Department of Defense, Washington Headquarters Services, Directorate for Information Operations and Reports (0704-0188), 1215 Jefferson Davis Highway, Suite 1204, Arlington, VA 22202-4302. Respondents should be aware that notwithstanding any other provision of law, no person shall be subject to any penalty for failing to comply with a collection of information if it does not display a currently valid OMB control number. **PLEASE DO NOT RETURN YOUR FORM TO THE ABOVE ADDRESS.**

1. REPORT DATE *(DD-MM-YYYY)*	2. REPORT TYPE	3. DATES COVERED *(From - To)*
March 2022	Final	

4. TITLE AND SUBTITLE

The Blowing Snow Hazard Assessment and Risk Prediction Model:

A Python Based Downscaling and Risk Prediction for Snow Surface Erodibility and Probability of Blowing Snow

5a. CONTRACT NUMBER

5b. GRANT NUMBER

5c. PROGRAM ELEMENT NUMBER
0603734A

6. AUTHOR(S)

Theodore W. Letcher, Sandra L. LeGrand and Chris Polashenski

5d. PROJECT NUMBER
479378

5e. TASK NUMBER
T15/RK17

5f. WORK UNIT NUMBER

7. PERFORMING ORGANIZATION NAME(S) AND ADDRESS(ES)

Cold Regions Research and Engineering Laboratory
U.S. Army Engineer Research and Development Center
72 Lyme Road
Hanover, NH 03755

8. PERFORMING ORGANIZATION REPORT NUMBER

ERDC/CRRELSR-22-1

9. SPONSORING / MONITORING AGENCY NAME(S) AND ADDRESS(ES)

Assistant Secretary of the Army for Acquisitions, Logistics, and Technology
103 Army Pentagon
Washington, DC 20314-1000

10. SPONSOR/MONITOR'S ACRONYM(S)

11. SPONSOR/MONITOR'S REPORT NUMBER(S)

12. DISTRIBUTION / AVAILABILITY STATEMENT
Approved for public release; distribution is unlimited.

13. SUPPLEMENTARY NOTES

Extreme Terrain Research, "Forecasting EO/IR Extinction Characteristics for Active and Passive Optical Systems" under Work Item BKCH02, Funding Account Number U4365315

14. ABSTRACT

Blowing snow is an extreme terrain hazard causing intermittent severe reductions in ground visibility and snow drifting. These hazards pose significant risk to operations in snow-covered regions. While many ingredients-based forecasting methods can be employed to predict where blowing snow is likely to occur, there are currently no physically based tools to predict blowing snow from a weather forecast. However, there are several different process models that simulate the transport of snow over short distances that can be adapted into a terrain forecasting tool. This report documents a downscaling and blowing-snow prediction tool that leverages existing frameworks for snow erodibility, lateral snow transport, and visibility, and applies these frameworks for terrain prediction. This tool is designed to work with standard numerical weather model output and user-specified geographic models to generate spatially variable forecasts of snow erodibility, blowing snow probability, and deterministic blowing-snow visibility near the ground. Critically, this tool aims to account for the history of the snow surface as it relates to erodibility, which further refines the blowing-snow risk output. Qualitative evaluations of this tool suggest that it can provide more precise forecasts of blowing snow. Critically, this tool can aid in mission planning by downscaling high-resolution gridded weather forecast data using even higher resolution terrain dataset, to make physically based predictions of blowing snow.

15. SUBJECT TERMS

Blowing snow	Extreme cold	Snow
Visibility	Weather prediction	Wind-snow interaction
	Cold regions – Weather	Snow erosion
	Blizzards -- Visibility	Winter storms -- Visibility

16. SECURITY CLASSIFICATION OF:			17. LIMITATION OF ABSTRACT	18. NUMBER OF PAGES	19a. NAME OF RESPONSIBLE PERSON
a. REPORT	b. ABSTRACT	c. THIS PAGE			19b. TELEPHONE NUMBER *(include area code)*
Unclassified	Unclassified	Unclassified	SAR	51	